Superconductivity in the Rh-based Heusler family $M\mathrm{Rh_2Sn}$

T. Klimczuk,[1,2,3] K. Gofryk,[1] C. H. Wang,[1,4] J. M. Allred,[5] F. Ronning,[1] W. Sadowski,[3] J.-C. Griveau,[2] E. Colineau,[2] D. Safarik,[1] J. D. Thompson,[1] and R. J. Cava[5]

[1]*Los Alamos National Laboratory, Los Alamos, New Mexico 87545, USA*

[2]*Joint Research Center, Institute for Transuranium Elements, European Commission, Postfach 2340, Karlsruhe D-76125, Germany*

[3]*Faculty of Applied Physics and Mathematics, Gdansk University of Technology, Narutowicza 11/12, 80-952 Gdansk, Poland*

[4]*University of California, Irvine, California 92697, USA*

[5]*Department of Chemistry, Princeton University, Princeton, New Jersey 08544, USA*

(Received 14 July 2010; revised manuscript received 15 September 2010; published 14 October 2010)

Superconductivity and structural characterization is reported for the Heusler structure compounds $\mathrm{ScRh_2Sn}$, $\mathrm{LuRh_2Sn}$, and $\mathrm{YRh_2Sn}$. The superconducting T_c's are 2.0 K, 2.9 K, and 4.1 K, respectively. The electronic contributions to the specific heat and the Debye temperatures are reported, and suggest that the observed trend in T_c is governed primarily by an increase in electron-phonon coupling on going from $\mathrm{ScRh_2Sn}$ to $\mathrm{YRh_2Sn}$. The electron-phonon coupling constant λ_{ep} and the normalized specific-heat jump $\Delta C/\gamma T_c$ suggest that the $M\mathrm{Rh_2Sn}$ system evolves from weak coupling to moderate coupling superconductivity.

DOI: 10.1103/PhysRevB.82.134520 PACS number(s): 74.70.Ad, 71.20.Be, 74.25.Bt

I. INTRODUCTION

A large number of ternary intermetallic compounds are known to form in the Heusler and half-Heusler structure types. These compounds display interesting physical properties, ranging from high Seebeck coefficient thermoelectrics,[1,2] to half metallic ferromagnets,[3,4] to superconductivity,[5–8] and have recently been proposed as hosts for topological surface states.[9,10] The prototype of the family, $\mathrm{AlCu_2Mn}$, was studied at the beginning of the last century by Friedrich Heusler.[11] The Heusler alloys, also called full Heuslers, crystallize in the cubic $L2_1$ structure and have the general formula AT_2M. In the formula, A stands for d transition metals such as Y, Sc, Ti, Hf, Zr, Nb, and Mn but some of the smallest rare-earth elements form the compound as well. T is a transition metal from groups VIIIB and IB of the periodic table and M stands for sp metals and the metalloids Sb and Bi.[12]

Among more than half-thousand reported Heusler compounds, fewer than 30 are superconductors, all with rather low transition temperatures. The Pd-based Heusler superconductors $\mathrm{YPd_2Sn}$, $\mathrm{LuPd_2Sn}$, and $\mathrm{ScPd_2Sn}$ are among the first discovered superconductors in this family.[5,13] Here we report that the analogous Rh-based compounds $\mathrm{YRh_2Sn}$, $\mathrm{LuRh_2Sn}$, and $\mathrm{ScRh_2Sn}$ are superconducting, with T_c's in the range of 2–4 K. We also report an elementary band-structure calculation for the Y-based compound. Comparison of the measured properties suggests that variation in the electron-phonon coupling in the series is an important factor in determining the observed trend in T_c.

II. EXPERIMENTAL

The polycrystalline samples were prepared by arc melting mixtures of the pure elements (2–5 % excess Sn was used to compensate for volatilization) in an ultrapure argon atmosphere. Special care was taken to avoid oxygen contamination. The samples were annealed afterward at 750 °C in evacuated quartz tubes. This temperature was held for a week before the tubes were quenched in −13 °C brine to minimize possible structural disorder.[8] The samples were characterized before and after annealing by powder x-ray diffraction, performed on a Scintag XDS 2000 diffractometer with Cu K_α radiation ($\lambda = 0.15460$ nm). Rietveld refinements of the structures were achieved using GSAS.[14,15]

dc magnetic measurements were performed using a commercial superconducting quantum interference device magnetometer (Quantum Design). ac magnetic measurements, heat capacity, and ac electrical resistivity (60 Hz) were measured in a Quantum Design Physical Property Measurement System. For the heat-capacity measurements, a standard relaxation calorimetry method was used. For the resistivity measurements we used a standard four-probe technique, with four platinum wires spot welded to the surface of previously polished samples. The electronic structure of $\mathrm{YPd_2Sn}$ was calculated using the full-potential linearized augmented plane-wave method in the elk implementation.[16] The generalized gradient approximation was used with parameters from Perdew, Burke, and Ernzerhof for the exchange-correlation functional.[17] A grid of $25\times25\times25$ points was used as the basis of the k-space vectors.

III. RESULTS AND DISCUSSION

A. Structural characterization

Both resistivity and magnetization tests indicate that for $\mathrm{ScRh_2Sn}$ and $\mathrm{LuRh_2Sn}$ the annealing process improves the superconducting properties and the crystallinity of the Heusler phase, whereas the same treatment for $\mathrm{YRh_2Sn}$ induces partial chemical decomposition of the Heusler phase and degrades the superconductivity. Therefore in this paper we present the physical and crystallographic properties of as-melted, quenched $\mathrm{YRh_2Sn}$, and annealed $\mathrm{ScRh_2Sn}$ and $\mathrm{LuRh_2Sn}$.

The $M\mathrm{Rh_2Sn}$ ($M=\mathrm{Sc,Y,Lu}$) compounds crystallize in the Heusler structure, shown in the inset of Fig. 1. In the cubic $L2_1$ Heusler structure, space group $Fm\bar{3}m$, the M atom oc-

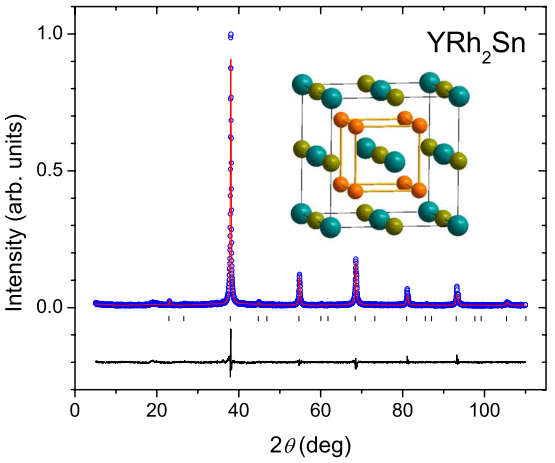

FIG. 1. (Color online) Observed (blue circles) and calculated (solid red line) powder x-ray diffraction pattern for YRh_2Sn at room temperature. The difference plot is shown at the bottom and vertical bars represent the Bragg peak positions for the cubic $L2_1$ Heusler structure. The inset shows the full Heusler-type crystal structure. Refined structural parameters for YRh_2Sn at 298 K: space group $Fm\bar{3}m$ (No. 225), $a=6.7139(2)$ Å, calculated density 9.1 gm cm^{-3}. Figures of merit: goodness of fit $(\chi^2)=1.83$, weighted profile residual $(R_{wp})=20\%$, profile residual $(R_p)=13\%$, and residual on structure factors $[R(F^2)]=10\%$.

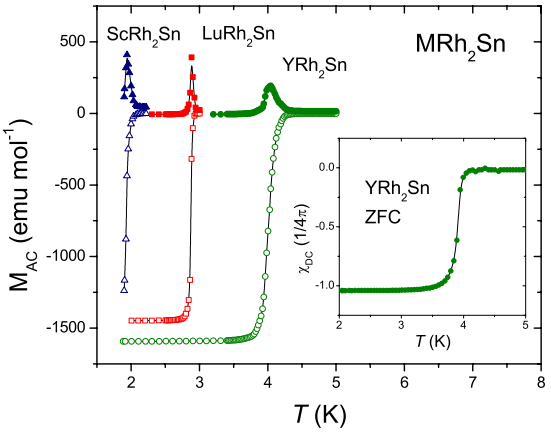

FIG. 2. (Color online) Temperature-dependent ac-susceptibility measurement for MRh_2Sn, where $M=$Sc, Lu, and Y. Open (filled) symbols is the real (imaginary) part of the ac susceptibility. The inset shows zero-field cooling dc susceptibility versus temperature for YRh_2Sn. The demagnetization factor was used as described in the text.

cupies site $4a$ $(0,0,0)$, Rh occupies site $8c$ $(\frac{1}{4},\frac{1}{4},\frac{1}{4})$, and Sn occupies site $4b$ $(\frac{1}{2},\frac{1}{2},\frac{1}{2})$. Figure 1 shows as an example the powder XRD pattern for as-cast YRh_2Sn; all atomic positions are fixed by symmetry and other structural parameters were freely refined in the fit. Refined lattice are 6.7139(2) Å, 6.6417(3) Å, and 6.5079(5) Å for YRh_2Sn, $LuRh_2Sn$, and $ScRh_2Sn$, respectively. These numbers are very close to the reported lattice parameters for the corresponding MPd_2Sn compounds.[13] The relative covalent radii of Y, Lu, and Sc account for the respective unit-cell sizes.

B. Properties of the superconducting state

The superconducting transition for all MRh_2Sn $(M=Y,Lu,Sc)$ samples was initially characterized via measurements of ac susceptibility. Figure 2 presents ac susceptibility versus temperature with the applied $\mu_0 H_{dc}$ field 0.5 mT and $\mu_0 H_{ac}$ field 0.3 mT. A very sharp onset of superconductivity (T_c) is observed for both $ScRh_2Sn$ and $LuRh_2Sn$, whereas for YRh_2Sn the transition is broader; ΔT_c is about 0.4 K. Table I summarizes crystallographic data and superconducting critical temperatures for MRh_2Sn and previously reported MPd_2Sn $(M=Y,Lu,Sc)$ compounds. Similarly to MPd_2Sn, the highest T_c is found for YRh_2Sn and decreases as the lattice parameter decreases on proceeding from Y to Lu to Sc. The same observation was made in the Pd-based phases[18] and for $Y_{\approx 1}Pd_2Sn_{\approx 1}$ under pressure.[19]

To estimate the demagnetization factor (d) for the studied samples, measurements of the low-field magnetization as a function of field $M(H)$ were performed at various temperatures below T_c. A representative measurement at 2 K for YRh_2Sn is shown in the main panel of Fig. 3. Assuming that the initial linear response to a magnetic field of less than 5 mT is perfectly diamagnetic, that is, that the slope dM/dH is $-1/4\pi$, we obtain a demagnetization factor that is consistent with the sample's shape. Applying this demagnetization factor, and calculating the volume of the sample (based on refined lattice parameter), gives the maximum observed zero-field cooling susceptibility of approximately $-1.02(1/4\pi)$ for YRh_2Sn. A somewhat smaller value, possibly caused by the presence of a small amount of impurities, was obtained for $LuRh_2Sn$ $[-0.92(1/4\pi)]$. Due to the low superconducting temperature for $ScRh_2Sn$, a similar analysis was not possible in that case.

As shown in the main panel of Fig. 3, $M(H)$ for YRh_2Sn, begins to deviate from a fitted linear dependence on $\mu_0 H$ at a field $\mu_0 H^*=6.2$ mT, giving a lower critical field, taking into account the demagnetization factor, of $\mu_0 H_{c1}(2\ \mathrm{K})=\mu_0 H^*/(1-d)\approx 7.0\pm 1.2$ mT. The estimated uncertainty reflects the criteria that $\mu_0 H^*$ is either the field above which M first deviates from the fitted line or the field where M deviates by 2.5% above the fitted curve. The resulting $\mu_0 H_{c1}$ vs T behavior is plotted in the inset of Fig. 3, allowing the estimation of $\mu_0 H_{c1}(0)$ for YRh_2Sn as 9.8 mT assuming the form $\mu_0 H_{c1}(T)=\mu_0 H_{c1}(0)[1-(T/T_c)^2]$.

The superconducting transition of MRh_2Sn was further examined through measurements of the electrical resistivity; the results are shown in the main panel of Fig. 4. The critical temperatures estimated from these measurements are very close to those estimated from $M_{ac}(T)$. A very sharp transition is visible for all compounds, an indication of the good quality of the samples. However, the normal-state resistivity measured just above T_c is almost 2.5 times larger for YRh_2Sn than it is for $LuRh_2Sn$ and $ScRh_2Sn$. This is likely caused by the fact that the YRh_2Sn sample was not annealed after melting, and some residual structural disorder remains present. Similarly, the reported residual resistivity ratio (RRR) is the smallest for YRh_2Sn, RRR=1.4, compared to RRR=2.4 and 2.1 for $LuRh_2Sn$ and $ScRh_2Sn$, respectively. These rather low values of RRR are typical for Heusler compound, in-

TABLE I. Comparison of the structural and electronic characteristics of superconducting Heusler compounds in the MT_2Sn family for M=Y, Lu, and Sc and T=Rh and Pd. Crystal structure: $MnCu_2Al$ type, space group $Fm\bar{3}m$, M in 4a (0,0,0), T in 8c $(\frac{1}{4},\frac{1}{4},\frac{1}{4})$, and Sn in 4$b$ $(\frac{1}{2},\frac{1}{2},\frac{1}{2})$.

	T=Rh				T=Pd			
	a (Å)	T_c (K)	γ (mJ/mol K^2)	Θ_D (K)	a (Å)	T_c (K)	γ (mJ/mol K^2)	Θ_D (K)
YT_2Sn	6.7139(2)	4.1	8.55(4)	219	6.716[a]	4.55[a]	8.05(5)[b]	179[b]
LuT_2Sn	6.6417(3)	2.9	6.74(5)	228	6.644[a]	3.05[a]	7.0(1)[b]	224[b]
ScT_2Sn	6.5079(5)	2.0	6.57(2)	282	6.503[a]	2.05[a]		232[c]

[a]Reference 13.
[b]Reference 21.
[c]Reference 19.

cluding the chemically distinct compound $ZrNi_2Ga$, where the estimated RRR is about 2.[7]

The upper critical-field values, H_{c2}, were determined from electrical resistivity measurements under various magnetic fields, presented in the inset of Fig. 5. As shown by the dashed line in Fig. 5, the temperature dependence of H_{c2} is well described by the Werthamer-Helfand-Hohenberg (WHH) expression for a dirty type-II superconductor,[20] giving $\mu_o H_{c2}(0)=1.2$ T for YRh_2Sn. Knowing the values of H_{c1} and H_{c2}, we can calculate several superconducting parameters for YRh_2Sn. Using the Ginzburg-Landau formula for coherence length $\xi_{GL}(0)=[\phi_o/2\pi H_{c2}(0)]^{1/2}$, where ϕ_o is the flux quantum $h/2e$, we find $\xi_{GL}(0)=16$ nm. With these results for $\xi_{GL}(0)$ and H_{c1}, the penetration depth, $\lambda_{GL}(0)=207$ nm is obtained from $\mu_0 H_{c1}=\frac{\Phi_0}{4\pi\lambda_{GL}^2}\ln\frac{\lambda_{GL}}{\xi_{GL}}$, and, hence the Ginzburg-Landau parameter $\kappa\approx 13$, which suggests that YRh_2Sn is a type-II superconductor.

The heat capacity measured through the superconducting transition is shown for all three compounds in Fig. 6. The bulk nature of superconductivity is confirmed by sharp, large anomalies at temperatures that are consistent with the T_c's determined by magnetic susceptibility and resistivity measurements. Measured heat capacities at an applied field of $\mu_0 H=3$ T, which exceeds the upper critical-field values, were fitted using the formula $C_p=\gamma T+\beta T^3+\delta T^5$ in which the first and two last parameters are attributed to electronic and lattice contribution to the specific heat, respectively. The extracted Sommerfeld coefficients, γ, are very close to the values obtained for the analogous compounds in the MPd_2Sn family,[19,21] and are in the range typical of the Heusler materials.

A simple Debye model for the phonon contribution to the specific heat dictates that β is related to the Debye temperature through $\Theta_D=(\frac{12\pi^4}{5\beta}nR)^{1/3}$, where $R=8.314$ J/mol K, and $n=4$ is the number of atoms in the formula unit. Using the observed values of β, we find that the Debye temperature is highest for $ScRh_2Sn$ ($\Theta_D=282$ K) and lowest for YRh_2Sn ($\Theta_D=219$ K), which deviates from a simple mass relationship because the Debye temperature of significantly heavier $LuRh_2Sn$ ($\Theta_D=228$ K) falls between these two values. This suggests the presence of relatively stiff Lu-Rh bonds. Interestingly, a similar trend is observed in the Pd-based Heusler superconductors.

With these results, assuming $\mu^*=0.13$, the electron-phonon coupling constant (λ_{ep}) can be calculated from the McMillan relation,[22]

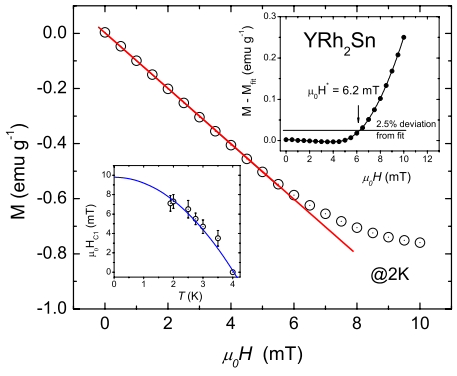

FIG. 3. (Color online) Field-dependent magnetization data $M(H)$ at constant temperature 2 K for YRh_2Sn. The red line corresponds to linear relation ($\sim\mu_0 H$) below 5.5 mT. The upper right inset shows deviation from a fitted linear dependence on $\mu_0 H$. The lower left inset is the temperature dependence of the lower critical field ($\mu_0 H_{c1}$) for YRh_2Sn.

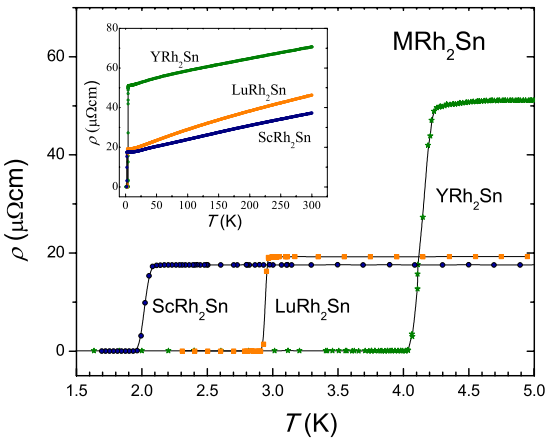

FIG. 4. (Color online) Electrical resistivity near superconducting transitions of MRh_2Sn, M=Sc, Lu, and Y, under zero field. The inset shows the resistivity measurement measured from 0.4 K to room temperature.

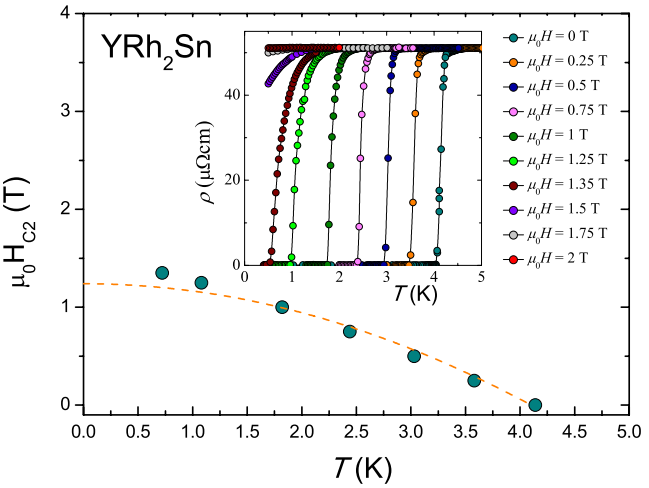

FIG. 5. (Color online) The upper critical field ($\mu_0 H_{C2}$) from resistivity as a function of temperature. The dashed curve is predicted by the WHH expression. The inset shows the YRh_2Sn low temperature resistivity [$\rho(T)$] for applied magnetic fields. Superconductivity vanishes for $\mu_0 H_C > 1.35$ T.

$$T_c = \frac{\Theta_D}{1.45}\exp\left[\frac{-1.04(1+\lambda_{ep})}{\lambda_{ep}-\mu^*(1+0.62\lambda_{ep})}\right].$$

By comparing the values of λ_{ep} obtained, we conclude that the MRh_2Sn system evolves from weak coupling to moderate coupling superconductivity, as λ_{ep} increases from 0.52 to 0.59 to 0.66 on proceeding from $ScRh_2Sn$ to $LuRh_2Sn$ to YRh_2Sn. Similarly, YRh_2Sn is more strongly correlated than the Lu analog when comparing their normalized specific-heat jumps $\Delta C/\gamma T_c$, a ratio that is often used as a test of the coupling strength.[23,24] The value $\lambda_{ep}=0.66$ obtained for YRh_2Sn is, to our knowledge, the highest reported for the Heusler compounds. Interestingly, taking the Debye temperature $\Theta_D=179$ K and the superconducting temperature $T_c=4.8$ K of YPd_2Sn (see Table I) we obtain an even higher

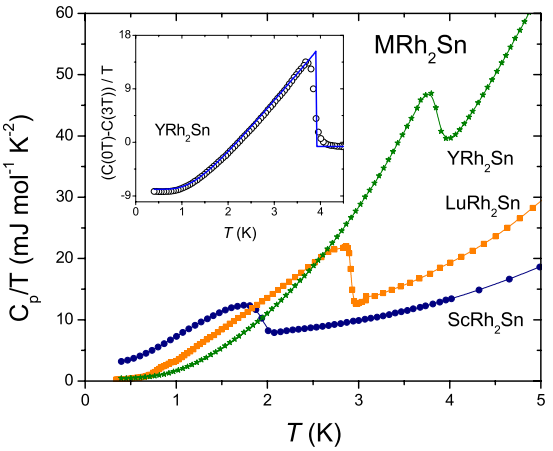

FIG. 6. (Color online) Zero-field specific heat divided by temperature (C_P/T) versus temperature for MRh_2Sn, where M=Sc, Lu, and Y. The inset shows raw experimental data for YRh_2Sn and blue solid line represents theoretical curve calculated based on BCS model with the *s*-wave gap as described in the text.

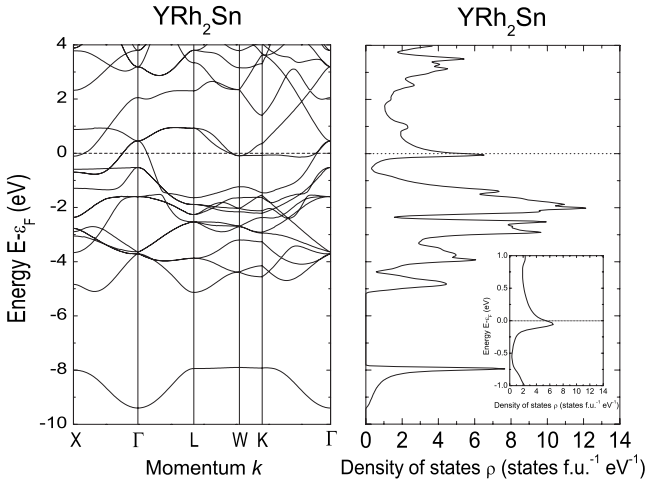

FIG. 7. Electronic structure (left) and corresponding DOS (right) of YRh_2Sn. Inset shows a detail of the DOS near Fermi energy, E_F.

$\lambda_{ep}=0.75$. This suggests that yttrium optimizes the electron-phonon coupling for superconductivity in Heusler phases.

In the framework of the free-electron gas, and including the enhancement of the Sommerfeld parameter by electron-phonon coupling, the density of states (DOS) at the Fermi energy can be calculated from: $N(E_F)=\frac{3}{\pi^2 k_B^2(1+\lambda_{ep})}\gamma$. The values obtained for all the MRh_2Sn (M=Sc, Y, Lu) compounds are almost the same [$N(E_F)\approx 2$ state/eV]. This means that a simple relationship between $N(E_F)$ and T_c is not found in this family as one might expect given the differences in λ_{ep}.

The specific-heat data shown in Fig. 6 provide additional information on the superconductivity in these materials. While the finite residual linear term seen in the $ScRh_2Sn$, could be taken as an indication of nodes or multiband superconducting gap behavior, it is more likely due to a sample which does not possess complete superconductivity. Independent of this, from the temperature dependence of the specific heat we can extract a value for the superconducting gap by fitting the data minus the phonons and the residual linear term to the expected BCS expectation,

$$C_{BCS} = t\frac{d}{dT}\int_0^\infty dy\left(\frac{-6\gamma\Delta_0}{k_B\pi}\right)[f\ln f+(1-f)\ln(1-f)],$$

where $t=T/T_c$, f is the Fermi function $f=1/(e^{E/k_BT}+1)$, $E=\sqrt{\varepsilon^2+\Delta^2}$, $y=\varepsilon/\Delta(0)$, and $\Delta(T)/\Delta(0)$ is taken from the tabulated values by Mühlschlegel.[25] The results for YRh_2Sn are shown in the inset of Fig. 6. The gap values are 0.70 meV, 0.44 meV, and 0.27 meV for YRh_2Sn, $LuRh_2Sn$, and $ScRh_2Sn$, respectively. This yields a ratio of $\Delta/k_BT_c=2.0$, 1.8, and 1.6, respectively, compared with the weak-coupling BCS expectation of 1.76 again indicating that YRh_2Sn is the strongest coupling superconductor of the three.

C. Band-structure calculations

The calculated band-structure results (Fig. 7) are very similar to those found for $ZrNi_2Ga$ (Ref. 7) but the Fermi level has moved down in a rigid-bandlike fashion to reflect

TABLE II. Characterization of the superconductivity in YRh_2Sn, $LuRh_2Sn$, and $ScRh_2Sn$.

	YRh_2Sn	$LuRh_2Sn$	$ScRh_2Sn$
T_c (K)	4.1	2.9	2
a (Å)	6.7139(2)	6.6417(3)	6.5079(5)
γ (mJ/mol K^2)	8.5	6.7	6.6
Θ_D (K)	219	228	282
$\Delta C/\gamma T_c$	1.7	1.49	
λ_{ep}	0.66	0.59	0.52
$N(E_F)$—experiment (states/eV/f.u.)	2.2	1.8	1.8
$N(E_F)$—calculations (states/eV/f.u.)	5.4	4.8	6.0
Δ (meV)	0.70	0.44	0.27
Δ/k_BT_c	2.0	1.8	1.6
$\mu_0H_{C1}(0)$ (mT)	9.8	7.5	
$\mu_0H_{C2}(0)$ (T)	1.26	0.50	0.30
ξ_{GL} (nm)	16.3	25.7	33
λ_{GL} (nm)	207	217	
κ	13	8	

the loss of 2 electrons/f.u.. This suggests that the superconducting state is more dependent on the general electronic features of the Heusler structure type than on the exact electronic count. The calculated $N(E_F)$'s of MRh_2Sn are 5.4, 4.8, and 6.0 (states eV^{-1} f.u.$^{-1}$) for Y, Lu, and Sc, respectively. The inset shows that the Fermi energy is predicted to be quite close to a peak in the DOS. Most of the electronic density around this peak is associated with a low dispersion band which is primarily Rh 4*d* in character and occurs along the path from W to K to Γ in the Brillouin zone. Small deviations in the dispersion of the contributing bands can move the Fermi level further or closer to the peak, which might explain the deviation in $N(E_F)_{MRh2Sn}/N(E_F)_{YRh2Sn}$ The calculated values are also more than twice larger than the measured values, indicating that in the actual compound the peak near $N(E_F)$ is probably shifted to a slightly higher energy, putting the actual E_F closer to the valley in DOS predicted by the band-structure calculations. Due to the sharpness of the peak in the DOS, a deviation of ~0.2 eV would reproduce the experimentally determined $N(E_F)$. This discrepancy could be caused by either a slight decrease in 4*d* band dispersion, which shifts more states toward the center of the band, or loss of <0.5 electron/f.u. which corresponds to ~2% vacancies on the Rh site.

IV. CONCLUSIONS

One of the predictions of the BCS theory is the relationship between the superconducting critical temperature and three material parameters: $T_c=1.13\Theta_D \exp[-1/VN(E_F)]$, where Θ_D is the Debye temperature, $N(E_F)$ is the density of states at the Fermi energy, and V is the electron-electron attractive interaction. Comparing the Debye temperatures for all six members of the MT_2Sn superconducting family (M=Sc,Y,Lu, T=Rh,Pd), we should expect the highest critical temperature for the compounds with the lightest M element: $ScRh_2Sn$ and $ScPd_2Sn$. However, the measured T_c's, as shown in the Table I, do not display this trend, which means that the Debye temperature is not the dominant parameter. The observed Sommerfeld parameters, a reflection of a dressed density of states $(1+\lambda_{ep})N(E_F)$, do, however trace the trend in T_c's.

As can be observed in Table II, the calculated $N(E_F)$ values increase by 18%, comparing values of $N(E_F)$ for YRh_2Sn and $ScRh_2Sn$, suggesting that the electronic structure can account for the observations. The last parameter to consider is the electron-electron attractive interaction (V), which in fact reflects the strength of the electron-phonon interaction in the material. We can compare this interaction through the electron phonon coupling constants (λ_{ep}). For MRh_2Sn, the superconducting critical temperature, T_c, increases as λ_{ep} increases. The relative change in λ_{ep} is 27% comparing the λ_{ep} values for YRh_2Sn and $ScRh_2Sn$. The same behavior can be deduced by comparing T_c and λ_{ep} for the $NbNi_2M$ (M=Al,Ga,Sn) family.[26]

For comparison purposes, we show in Table III various superconducting parameters for YRh_2Sn and the two strong-coupling superconductors Nb_3Sn and MgB_2. Comparing the numbers helps to explain why T_c in the Heusler system is relatively low. Although the Debye temperatures for Nb_3Sn

TABLE III. Comparison of superconducting parameters for YRh_2Sn, Nb_3Sn, and MgB_2.

	YRh_2Sn	Nb_3Sn	MgB_2
T_c (K)	4.1	17.8	36.7
γ (mJ/mol K^2)	8.5	54.8	2.7
$\Theta_D(0)$ (K)	219	234	6630[a]
λ_{ep}	0.66	1.34	1.07

[a]Debye temperature as the prefactor in the equation for T_c in the BCS theory is replaced by the energy of the E_{2g} optical phonon =570 meV (Ref. 27). Data for Nb_3Sn are compiled from Ref. 28; MgB_2 from Ref. 29.

and YRh_2Sn are almost identical, both the electron-phonon coupling constant and the Sommerfeld parameter are much lower (by a factor of 2) for the latter. Interestingly MgB_2 has smaller Sommerfeld parameter in comparison to YRh_2Sn, but the characteristic energy, which replaces Debye temperature,[27] is 30 times larger, resulting in a T_c that is almost ten times higher.

In conclusion, in the Heusler family, the trends in superconducting T_c appear to be driven primarily by the electron-phonon coupling. Comparing the values of λ_{ep} and the normalized specific-heat jump $\Delta C/\gamma T_c$ suggests that the MRh_2Sn system evolves from weak coupling to moderate coupling superconductivity.

ACKNOWLEDGMENTS

Work at Los Alamos National Laboratory was performed under the auspices of the U.S. Department of Energy, Office of Science. The work at Princeton University was supported by the U.S. Department of Energy, Grant No. DE-FG02-98ER45706. T.K. acknowledges the European Commission for financial support.

[1] C. Uher, J. Yang, S. Hu, D. T. Morelli, and G. P. Meisner, Phys. Rev. B **59**, 8615 (1999).
[2] H. Hohl, A. P. Ramirez, C. Goldmann, G. Ernst, B. Wölfing, and E. Bucher, J. Phys.: Condens. Matter **11**, 1697 (1999).
[3] R. Shan, H. Sukegawa, W. H. Wang, M. Kodzuka, T. Furubayashi, T. Ohkubo, S. Mitani, K. Inomata, and K. Hono, Phys. Rev. Lett. **102**, 246601 (2009).
[4] K. Hamaya, H. Itoh, O. Nakatsuka, K. Ueda, K. Yamamoto, M. Itakura, T. Taniyama, T. Ono, and M. Miyao, Phys. Rev. Lett. **102**, 137204 (2009).
[5] M. Ishikawa, J. L. Jorda, and A. Junod, *Superconductivity in d- and f-band Metals*, edited by W. Buckel and W. Weber (Kernforschungszentrum Karlsruhe, Germany, 1982).
[6] C. L. Seaman, N. R. Dilley, M. C. de Andrade, J. Herrmann, M. B. Maple, and Z. Fisk, Phys. Rev. B **53**, 2651 (1996).
[7] J. Winterlik, G. H. Fecher, C. Felser, M. Jourdan, K. Grube, F. Hardy, H. von Löhneysen, K. L. Holman, and R. J. Cava, Phys. Rev. B **78**, 184506 (2008).
[8] J. Winterlik, G. H. Fecher, A. Thomas, and C. Felser, Phys. Rev. B **79**, 064508 (2009).
[9] H. Lin, L. A. Wray, Y. Xia, S. Xu, S. Jia, R. J. Cava, A. Bansil, and M. Z. Hasan, Nature Mater. **9**, 546 (2010).
[10] S. Chadov, X. L. Qi, J. Kübler, G. H. Fecher, C. Felser, and S. C. Zhang, Nature Mater. **9**, 541 (2010).
[11] F. Heusler, Verh. Dtsch. Phys. Ges. **5**, 219 (1903).
[12] K. Gofryk, D. Kaczorowski, T. Plackowski, A. Leithe-Jasper, and Yu. Grin, Phys. Rev. B **72**, 094409 (2005).
[13] S. K. Malik, A. M. Umarji, and G. K. Shenoy, Phys. Rev. B **32**, 4426 (1985).
[14] B. H. Toby, J. Appl. Crystallogr. **34**, 210 (2001).
[15] A. C. Larson and R. B. Von Dreele, Los Alamos National Laboratory Report No. LAUR 86, 2000 (unpublished).
[16] http://elk.sourceforge.net/
[17] J. P. Perdew, K. Burke, and M. Ernzerhof, Phys. Rev. Lett. **77**, 3865 (1996).
[18] J. L. Jorda, M. Ishikawa, and J. Muller, J. Less-Common Met. **107**, 321 (1985).
[19] M. J. Johnson and R. N. Shelton, Solid State Commun. **52**, 839 (1984).
[20] N. R. Werthamer, E. Helfand, and P. Hohenberg, Phys. Rev. **147**, 295 (1966).
[21] T. Klimczuk (unpublished).
[22] W. L. McMillan, Phys. Rev. **167**, 331 (1968), we assumed the Coulomb coupling constant $\mu^*=0.13$.
[23] J. Teyssier, R. Lortz, A. Petrovic, D. van der Marel, V. Filippov, and N. Shitsevalova, Phys. Rev. B **78**, 134504 (2008).
[24] We do not evaluate the Sc analog in this manner due to the finite residual linear term and width of the superconducting transition.
[25] B. Mühlschlegel, Z. Phys. **155**, 313 (1959).
[26] S. Waki, Y. Yamaguchi, and K. Mitsugi, J. Phys. Soc. Jpn. **54**, 1673 (1985).
[27] J. M. An and W. E. Pickett, Phys. Rev. Lett. **86**, 4366 (2001).
[28] V. Guritanu, W. Goldacker, F. Bouquet, Y. Wang, R. Lortz, G. Goll, and A. Junod, Phys. Rev. B **70**, 184526 (2004).
[29] Y. Wang, T. Plackowski, and A. Junod, Physica C **355**, 179 (2001).